



# Design and implementation of a dual-stage actuated HDD servo system via composite nonlinear control approach

Kemao Peng, Ben M. Chen<sup>\*</sup>, Tong H. Lee  
V. Venkataramanan

*Department of Electrical and Computer Engineering, The National University of Singapore,  
Singapore 117576, Singapore*

Accepted 28 May 2004

---

## Abstract

We consider in this paper the design and implementation of a dual-stage actuated hard disk drive (HDD) servo system, in which an additional piezoelectric actuator is mounted on top of the conventional voice-coil-motor (VCM) actuator to provide a faster and finer response. More specifically, the dual-stage actuated HDD servo system consists of a primary VCM actuator and a secondary suspension piezoelectric microactuator. The VCM actuator is used to quickly move the read/write (R/W) head of the HDD servo system to a target track, whereas the microactuator is used to fine-tune the R/W head position when it is getting closer to the target. In our design, the primary actuator is controlled by a newly developed composite nonlinear feedback (CNF) control law, which has fast rise time and small overshoot, and the microactuator is controlled through a simple static gain together with a low-pass filter and a notch filter. Simulation and implementation results show that in track following, the dual-stage actuated HDD servo system has outperformed the single-stage actuated counterpart by more than 47% in settling time and by 39% in position error signal (PES) tests.

© 2004 Elsevier Ltd. All rights reserved.

---

<sup>\*</sup> Corresponding author. Tel.: +65 6874 2289; fax: +65 6779 1103.

E-mail addresses: [elepkm@nus.edu.sg](mailto:elepkm@nus.edu.sg) (K. Peng), [bmchen@nus.edu.sg](mailto:bmchen@nus.edu.sg) (B.M. Chen), [eleleeth@nus.edu.sg](mailto:eleleeth@nus.edu.sg) (T.H. Lee), [engp7992@nus.edu.sg](mailto:engp7992@nus.edu.sg) (V. Venkataramanan).

Keywords: Actuators; Hard disk drives; Servo systems; Nonlinear control

### 1. Introduction

Hard disk drives (HDD) provide important data-storage medium for computers and other data-processing systems. Data in an HDD are arranged in concentric circles or tracks and are read or written with a read/write (R/W) head. The two main functions of the head positioning servomechanism in disk drives are track seeking and track following. Track seeking moves the R/W head from the present track to a specified destination track in minimum time using a bounded control effort. Track following maintains the head as close as possible to the destination track center while information is being read from or written to the disk. The prevalent trend in hard disk design is toward smaller hard disks with increasingly larger capacities. One of the limitations in the conventional disk drives to achieve higher data capacity is its bandwidth. That is, the voice-coil-motor (VCM) actuator used in conventional disk drives has hundreds of flexible resonant modes in high frequencies (see e.g., [8,25]). This limits the increase of bandwidth and hence the track density. A possible solution to this kind of problems is to introduce an additional microactuator on top of the conventional VCM actuator to provide a faster response and thus improve the overall servo performance in the track following stage. In fact, there is a considerable amount of research works that have been done along this line (see e.g., [1–3,5,6,9–17,19–23]).

Dual-stage actuator refers to the fact that there is a small twin-piezo actuator mounted between the base plate and active suspension of a large conventional VCM actuator. The R/W head is mounted at the end of the active suspension. Fig. 1 shows a simple illustration of a dual-stage actuator considered in this paper. The piezoelectric actuator or microactuator, driven by voltage, will only be activated in the track following stage because of its limited movement range. The microactuator produces relative motion of the R/W head along the active suspension or the radial direction in the center of the pivot (see e.g., [6,9]), while the VCM actuator rotates the base plate and active suspension to move the microactuator and the R/W head.

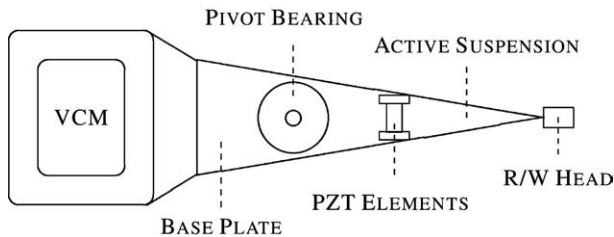


Fig. 1. A dual-stage HDD actuator.

Diverse control strategies and methods have been reported to design the dual-stage actuated HDD servo systems (see e.g., [5,9,12,13,15,17,19,21]). Guo et al. [9] have proposed four control strategies to design the dual-stage actuated control system, which are respectively the so-called parallel loop, master-slave loop, dual feedback loop and master-slave with decoupling methods. Guo et al. [12] and Hu et al. [15] have also utilized the well-known LQG/LTR method to design the dual-stage actuated HDD servo systems. These works have accelerated the progress to improve the HDD servo system performance. But, more studies on the control methods need to be conducted to achieve better results and higher track density in HDD servo systems.

In this paper, we will primarily focus on the design of a dual-stage actuated HDD control system using a newly developed composite nonlinear feedback (CNF) control technique. The CNF control law, which consists of a linear component and a nonlinear component in its control signal, is capable of tracking a large magnitude set point with faster speed and smaller overshoot. The technique was originally proposed by Lin et al. [18] for a class of second-order systems with state feedback. It has recently been extended by Chen et al. [4] to general linear systems with measurement feedback. It has been shown in [4] that the CNF technique yields a much better performance compared to that of the conventional proximate time-optimal servomechanism (PTOS) in single-stage actuated HDD. More importantly, it does not require any switching element in between the track seeking mode and the track following mode. In our design, the VCM actuator will be controlled by a CNF control law, and the microactuator will be controlled by a static gain together with a fourth-order filter, which is used to attenuate high frequency resonance modes and noises. These two controllers will then be combined to yield a complete dual-stage actuated HDD servo system applicable for both the track seeking and track following stages. Our results show that dual-stage actuated HDD servo system has outperformed the single-stage counterpart a great deal.

The paper is organized as follows. Section 2 deals with the identification of the mathematical models of the VCM actuator and microactuator, which are used to form the dual-actuated HDD servo system. We will recall the detailed design procedure of the reduced-order CNF controller in Section 3, which will then be utilized to design the dual-stage actuated HDD servo system in Section 4. The simulation and implementation results of the single-stage and dual-stage actuated systems will be presented and compared in Section 5. Finally, we draw the conclusion of our work in Section 6.

## **2. Modeling of the dual-stage actuated HDD system**

In this section, the mathematical models of the VCM actuator and the microactuator are derived to compose the model of the dual-stage actuated HDD servo system. These models are identified through frequency response characteristics obtained from experiment using a laser Doppler vibrometer (LDV) and a dynamic signal analyzer. We would like to note that in our experimental setup, the cover of the hard

disk drive and the disk plates are removed. The displacement of the HDD R/W head is measured by the LDV. The frequency responses are measured for the two actuators one by one with the input signal to the other actuator being set to zero. The frequency response characteristics of the VCM actuator and the microactuator used in our experiment are respectively shown in Figs. 2 and 3. Using these measured data from the actual system, and the algorithms of [7,24], we obtain a tenth order model for the VCM actuator together with its driver and a converter from voltage to electric current,

$$\begin{aligned}
 G_v(s) = & \frac{6.4013 \times 10^7}{s^2} \cdot \frac{0.912s^2 + 457.4s + 1.433 \times 10^8}{s^2 + 359.2s + 1.433 \times 10^8} \\
 & \cdot \frac{0.7586s^2 + 962.2s + 2.491 \times 10^8}{s^2 + 789.1s + 2.491 \times 10^8} \cdot \frac{9.917 \times 10^8}{s^2 + 1575s + 9.917 \times 10^8} \\
 & \cdot \frac{2.731 \times 10^9}{s^2 + 2613s + 2.731 \times 10^9}, \tag{1}
 \end{aligned}$$

whose input  $u_v$  is in volts with  $|u_v| \leq 3$  volts. The output  $y_v$  is in  $\mu\text{m}$ . We obtain also a tenth order model for the microactuator together with its driver and a linear amplifier from voltage to voltage,

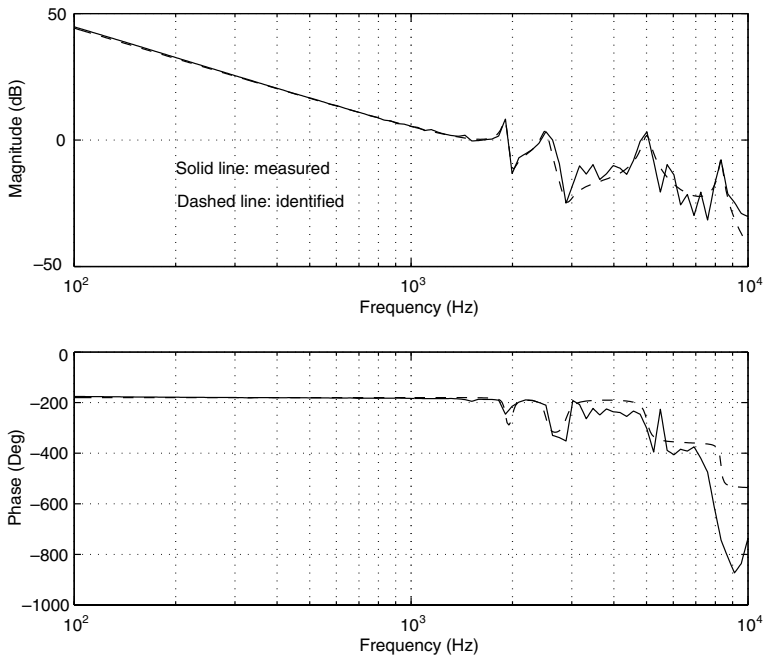


Fig. 2. Frequency response characteristics of the VCM actuator.

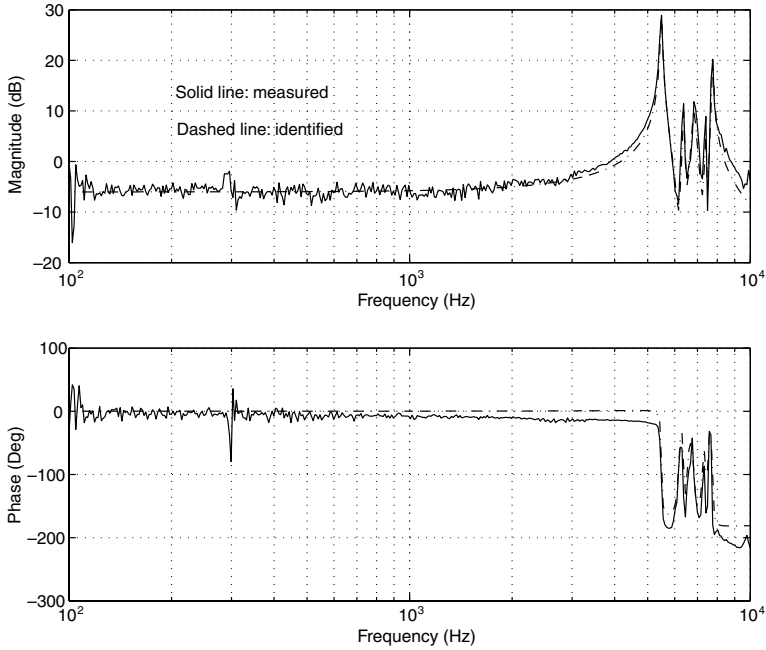


Fig. 3. Frequency response characteristics of the microactuator.

$$\begin{aligned}
 G_m(s) = & 0.5 \times \frac{0.7938s^2 + 767.9s + 1.189 \times 10^9}{s^2 + 344.8s + 1.189 \times 10^9} \\
 & \cdot \frac{0.955s^2 + 978.6s + 1.605 \times 10^9}{s^2 + 400.6s + 1.605 \times 10^9} \cdot \frac{0.8912s^2 + 1013s + 1.843 \times 10^9}{s^2 + 1073s + 1.843 \times 10^9} \\
 & \cdot \frac{0.9772s^2 + 460.1s + 2.167 \times 10^9}{s^2 + 465.5s + 2.167 \times 10^9} \cdot \frac{2.376 \times 10^9}{s^2 + 487.4s + 2.376 \times 10^9}, \quad (2)
 \end{aligned}$$

in which the input  $u_m$  is again in volts with  $|u_m| \leq 2$  volts. The output  $y_m$  is again in  $\mu\text{m}$ . The only measurement output for the whole system,  $y$ , is the combination of  $y_v$  and  $y_m$ , i.e.,

$$y = y_v + y_m. \quad (3)$$

We note that in practical situations, it is required to design a single servo controller that works for a whole batch of drives with resonance modes varying from drive to drive. As such, we have to design a controller that is robust enough to cope with different resonance modes. Also, in order to simplify our design procedure, we first set aside the resonance modes and approximate the model of the VCM actuator as follows:

$$\Sigma_v : \begin{cases} \dot{x}_v = \begin{bmatrix} 0 & 1 \\ 0 & 0 \end{bmatrix} x_v + \begin{bmatrix} 0 \\ 6.4013 \times 10^7 \end{bmatrix} \text{sat}(u_v), \\ y_v = [1 \quad 0] x_v, \end{cases} \quad (4)$$

and by adding appropriate filters, the microactuator model can be approximated as

$$\Sigma_m : y_m = 0.5 \text{sat}(u_m). \tag{5}$$

It can be seen soon that such approximations on the actuator models are working perfectly in our design. We would like to note that the simulation results obtained in Section 5 are actually done using the models with resonance modes, i.e., the models in (1) and (2).

### 3. Reduced order composite nonlinear feedback control

In this section, we recall from Chen et al. [4] the procedure of designing a reduced order composite nonlinear feedback (CNF) control technique for a class of linear systems with actuator saturation. The CNF control consists of a linear feedback law and a nonlinear feedback law without any switching element. The linear feedback part is designed to yield a closed-loop system with a small damping ratio for a quick response, while at the same time not exceeding the actuator limits for the desired command input levels. The nonlinear feedback law is used to increase the damping ratio of the closed-loop system as the system output approaches the target reference to reduce the overshoot caused by the linear part.

More specifically, we consider a linear continuous-time system  $\Sigma$  with an amplitude-constrained actuator characterized by

$$\begin{cases} \dot{x} = Ax + B \text{sat}(u), & x(0) = x_0, \\ y = C_1 x, \\ h = C_2 x, \end{cases} \tag{6}$$

where  $x \in \mathbb{R}^n$ ,  $u \in \mathbb{R}$ ,  $y \in \mathbb{R}^p$  and  $h \in \mathbb{R}$  are respectively the state, control input, measurement output and controlled output of  $\Sigma$ .  $A$ ,  $B$ ,  $C_1$  and  $C_2$  are appropriate dimensional constant matrices, and  $\text{sat} : \mathbb{R} \rightarrow \mathbb{R}$  represents the actuator saturation defined as

$$\text{sat}(u) = \text{sgn}(u) \min\{u_{\max}, |u|\}, \tag{7}$$

with  $u_{\max}$  being the saturation level of the input. The following assumptions on the system are required: (i)  $(A, B)$  is stabilizable; (ii)  $(A, C_1)$  is detectable; and (iii)  $(A, B, C_2)$  is invertible and has no invariant zeros at  $s = 0$ .

The objective of this section is to design a reduced order CNF control law that will cause the controlled output to track a high amplitude step input rapidly without experiencing large overshoot and without the adverse actuator saturation effects. This will be done through the design of a linear feedback law with a small closed-loop damping ratio and a nonlinear feedback law through an appropriate Lyapunov function to cause the closed-loop system to be highly damped as system output approaches the command input to reduce the overshoot.

For the given system in (6), it is clear that there are  $p$  state variables of the system measurable if  $C_1$  is of maximal rank. Thus, in general, it is not necessary to estimate these measurable state variables in measurement feedback laws. As such, we will design a dynamic controller that has a dynamical order less than that of the given

plant. We now proceed to construct such a control law under the CNF control framework.

For simplicity of presentation, we assume that  $C_1$  is already in the form

$$C_1 = [I_p \ 0]. \tag{8}$$

Then, the system in (6) can be rewritten as

$$\begin{cases} \begin{pmatrix} \dot{x}_1 \\ \dot{x}_2 \end{pmatrix} = \begin{bmatrix} A_{11} & A_{12} \\ A_{21} & A_{22} \end{bmatrix} \begin{pmatrix} x_1 \\ x_2 \end{pmatrix} + \begin{bmatrix} B_1 \\ B_2 \end{bmatrix} \text{sat}(u), & x_0 = \begin{pmatrix} x_{10} \\ x_{20} \end{pmatrix}, \\ y = [I_p \ 0] \begin{pmatrix} x_1 \\ x_2 \end{pmatrix}, \\ h = C_2 \begin{pmatrix} x_1 \\ x_2 \end{pmatrix}, \end{cases} \tag{9}$$

where the original state  $x$  is partitioned into two parts,  $x_1$  and  $x_2$  with  $y \equiv x_1$ . Thus, we will only need to estimate  $x_2$  in the reduced order measurement feedback design. Next, we let  $F$  be chosen such that (i)  $A + BF$  is asymptotically stable, and (ii)  $C_2(sI - A - BF)^{-1}B$  has desired properties, i.e., it has a small damping ratio with a quick rise time, and let  $K_R$  be chosen such that  $A_{22} + K_R A_{12}$  is asymptotically stable. Here we note that it can be shown that  $(A_{22}, A_{12})$  is detectable if and only if  $(A, C_1)$  is detectable. Thus, there exists a stabilizing  $K_R$ . Again, such  $F$  and  $K_R$  can be designed using usual linear control techniques. We then partition  $F$  in conformity with  $x_1$  and  $x_2$ ,

$$F = [F_1 \ F_2]. \tag{10}$$

and define

$$G = -[C_2(A + BF)^{-1}B]^{-1}, \quad H = [1 - F(A + BF)^{-1}B]G, \tag{11}$$

and

$$x_e = -(A + BF)^{-1}BGr, \tag{12}$$

where  $r$  is the command reference signal. Next, given a positive definite matrix  $W \in \mathbb{R}^{n \times n}$ , let  $P > 0$  be the solution to the Lyapunov equation

$$(A + BF)'P + P(A + BF) = -W. \tag{13}$$

Given another positive definite matrix  $W_R \in \mathbb{R}^{(n-p) \times (n-p)}$  with

$$W_R > F_2' B' P W^{-1} P B F_2, \tag{14}$$

let  $Q_R > 0$  be the solution to the Lyapunov equation

$$(A_{22} + K_R A_{12})' Q_R + Q_R (A_{22} + K_R A_{12}) = -W_R. \tag{15}$$

Note that such  $P$  and  $Q_R$  exist as  $A + BF$  and  $A_{22} + K_R A_{12}$  are asymptotically stable.

The reduced order CNF controller is given by

$$\dot{x}_c = (A_{22} + K_R A_{12})x_c + [A_{21} + K_R A_{11} - (A_{22} + K_R A_{12})K_R]y + (B_2 + K_R B_1) \text{sat}(u) \tag{16}$$

and

$$u = F \left[ \begin{pmatrix} y \\ x_c - K_{RY} \end{pmatrix} - x_e \right] + Hr + \rho(r, y) B'P \left[ \begin{pmatrix} y \\ x_c - K_{RY} \end{pmatrix} - x_e \right], \tag{17}$$

where  $\rho(r, y)$  is a non-positive scalar function locally Lipschitz in  $y$  subject to certain constraints to be discussed later.

For any  $\delta \in (0, 1)$ , let  $c_\delta$  be the largest positive scalar such that for all

$$\begin{pmatrix} x \\ x_c \end{pmatrix} \in X_{R\delta} := \left\{ \begin{pmatrix} x \\ x_c \end{pmatrix} : \begin{pmatrix} x \\ x_c \end{pmatrix}' \begin{bmatrix} P & 0 \\ 0 & Q_R \end{bmatrix} \begin{pmatrix} x \\ x_c \end{pmatrix} \leq c_\delta \right\}, \tag{18}$$

we have

$$\left| [F \quad F_2] \begin{pmatrix} x \\ x_c \end{pmatrix} \right| \leq u_{\max}(1 - \delta). \tag{19}$$

We have the following theorem. The proof of the theorem follows pretty closely from the full order measurement feedback case reported in [4].

**Theorem 3.1.** *Consider the given system in (6). Then, there exists a scalar  $\rho^* > 0$  such that for any non-positive function  $\rho(r, y)$ , locally Lipschitz in  $y$  and  $|\rho(r, y)| \leq \rho^*$ , the reduced order CNF law given by (16) and (17) will drive the system controlled output  $h(t)$  to track asymptotically the step command input of amplitude  $r$  from an initial state  $x_0$ , provided that  $x_0$ ,  $x_{c0}$  and  $r$  satisfy*

$$\begin{pmatrix} x_0 - x_e \\ x_{c0} - x_{20} - K_R x_{10} \end{pmatrix} \in X_{R\delta} \quad \text{and} \quad |Hr| \leq \delta \cdot u_{\max}. \tag{20}$$

The freedom to choose the function  $\rho(r, y)$  is used to tune the control laws so as to improve the performance of the closed-loop system as the controlled output  $h$  approaches the set point. Since the main purpose of adding the nonlinear part to the CNF controllers is to speed up the settling time, or equivalently to contribute a significant value to the control input when the tracking error,  $r - h$ , is small. The nonlinear part, in general, will be in action when the control signal is far away from its saturation level, and thus it will not cause the control input to hit its limits. Under such a circumstance, it is straightforward to verify that the closed-loop system comprising the given plant in (6) and the reduced order CNF control law can be expressed as

$$\dot{\tilde{x}} = (A + BF)\tilde{x} + \rho(r, y)BB'P\tilde{x}. \tag{21}$$

We note that the additional term  $\rho(r, y)$  does not affect the stability of the estimators. It is now clear that eigenvalues of the closed-loop system in (21) can be changed by the function  $\rho(r, y)$ . In what follows, we proceed to interpret the closed-loop system of (21) using the classical feedback control concept as given in Fig. 4, where the auxiliary system  $G_{\text{aux}}(s)$  is defined as

$$G_{\text{aux}}(s) := C_{\text{aux}}(sI - A_{\text{aux}})^{-1}B_{\text{aux}} := B'P(sI - A - BF)^{-1}B. \tag{22}$$

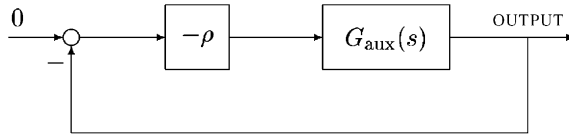


Fig. 4. Interpretation of the nonlinear function  $\rho(r, y)$ .

It has been proved in Chen et al. [4] that  $G_{aux}(s)$  is stable and invertible with a relative degree equal to 1, and is of minimum phase with  $n - 1$  stable invariant zeros.

It is clear that the invariant zeros of  $G_{aux}(s)$  play an important role in selecting the poles of the closed-loop system of (21). The poles of the closed-loop system approach the locations of the invariant zeros of  $G_{aux}(s)$  as  $|\rho|$  becomes larger and larger. We would like to note that there is freedom in pre-selecting the locations of these invariant zeros. This can actually be done by selecting an appropriate  $W > 0$  in (13). In general, we should select the invariant zeros of  $G_{aux}(s)$ , which are corresponding to the closed-loop poles for larger  $|\rho|$ , such that the dominated ones have a large damping ratio, which in turn will yield a smaller overshoot. We refer interested readers to [4] for a detailed guideline for the selection of an appropriate  $W$ . The selection of the nonlinear function  $\rho(r, y)$  is relatively simple once the desired invariant zeros of  $G_{aux}(s)$  are obtained. We usually choose  $\rho$  as a function of the tracking error, i.e.,  $r - h$ , which in most practical situations is known and available for feedback. The following choice of  $\rho$ , an exponential function, has been tested to be working very well,

$$\rho(r, h) = -\beta |e^{-\alpha|r-h|} - e^{-\alpha|r-h_0|}|, \tag{23}$$

where  $h_0 = h(0)$ , and  $\alpha > 0$  and  $\beta \geq 0$  are tuning parameters. This function  $\rho(r, h)$  changes from 0 to  $-\beta^* = -\beta |1 - e^{-\alpha|r-h_0|}|$  as the tracking error approaches zero. At the initial stage, when the controlled output  $h$  is far away from the final set point,  $\rho(r, h)$  is small and the effect of the nonlinear part on the overall system is very limited. When the controlled output  $h$  approaches the set point,  $\rho(r, h) \approx -\beta^*$ , and the nonlinear control law will become effective. In general, the parameter  $\beta$  should be chosen such that the poles of  $A + BF - \beta^* BB'P$  are in the desired locations, e.g., the dominated poles should have a large damping ratio. Finally, we note that the choice of  $\rho(r, h)$  is nonunique. Any continuous function would work so long as it has similar properties of that given in (23).

#### 4. Design of the dual-stage actuated HDD servo system

We now carry out the design of servo systems for the HDD with a dual-stage actuator. We would like to design our servo systems to the following requirements:

1. The control input to the VCM actuator should not exceed  $\pm 3$  V, whereas the control input to the microactuator should be within  $\pm 2$  V.
2. The displacement of the microactuator should not exceed 1  $\mu\text{m}$ . Moreover, it should settle down to zero in the steady state so that the microactuator can be further used for the next move.

3. The overshoot and undershoot of the step response should be kept less than 0.05  $\mu\text{m}$ , i.e., 5% of one track pitch. The R/W head of the HDD servo system can start reading or writing data on to the disk when it is within 5% of one track pitch of the target.
4. The resulting gain margin should be larger than 6 dB and the phase margin should be more than  $50^\circ$ .

Unfortunately, the only available measurement in the dual-stage actuated HDD is the displacement of the R/W head, which is a combination of the displacement of the VCM actuator and that of the microactuator. Practically, we have to control both actuators using a single measurement, which makes the servo system design very difficult. Observing the frequency response of the microactuator in Fig. 3, we find that it can in fact be approximated by a constant gain at low frequencies. This property will be valid so long as we do not push the speed of the microactuator too fast. As such, we propose in Fig. 5 a control configuration for the dual-stage actuated HDD servo system.

To be more specific, we estimate the displacement of the microactuator  $\hat{y}_m$  directly from its input  $u_m$  and then the estimation of the displacement of the VCM actuator can be obtained as  $y - \hat{y}_m$ . In the control configuration of Fig. 5, a reduced order CNF control law is adopted to control the VCM actuator. We note that for this particular problem, the controlled output and the measurement output are actually identical. It is obvious to observe from the simplified model of the VCM actuator in (4) that all the three assumptions of the previous section for the CNF technique are satisfied, and hence, it is safe to apply the technique to design a control law for the VCM actuator. A low-pass filter together with a notch filter are added on the path to the control input of the microactuator. The main purpose of adding these filters is to reduce the effects of the resonant modes of the microactuator and noises. The switch on the same path is to make sure that the microactuator is only to be activated when the tracking error is within the reach of the microactuator, which has a maximum displacement of 1  $\mu\text{m}$ . Our design philosophy is actually rather simple.

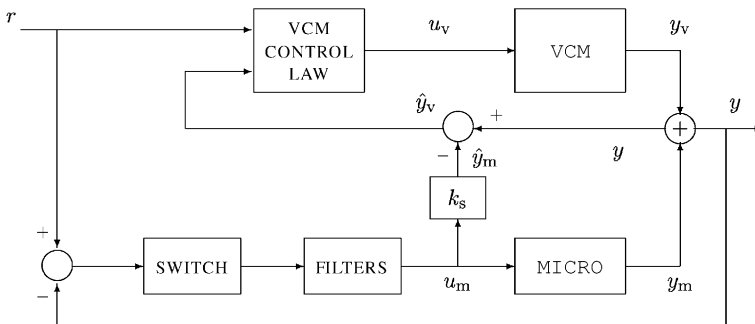


Fig. 5. The schematic representation of a dual-stage actuator control.

1. Since the maximum displacement of the microactuator is 1 μm, it will not provide much help in the track seeking stage. Thus, when the tracking error is large, i.e., the displacement  $y$  is far away from the target, the switch in the microactuator path will be turned off and only the VCM actuator will be solo in action.
2. When the R/W head is entering the target region, e.g., within 1 μm of the target reference, the switch will be turned on and the microactuator will be in action to speed up the response of the overall system.
3. It can be observed from the configuration in Fig. 5 that  $y_m$ , the displacement of the microactuator, will settle down to zero as the tracking error approaches zero. As pointed out earlier, such a feature would enable the microactuator to be used for the next move.

The detailed control parameters are as follows:

1. The switch is chosen such that the path is activated when  $|r - \hat{y}_v| \leq 1.5 \mu\text{m}$ . Otherwise, it will be open. we employ the following switching function:

$$\text{SWITCH FUNCTION} := \begin{cases} 0, & |r - y| > 1.5, \\ 1, & |r - y| \leq 1.5. \end{cases} \tag{24}$$

2. A low-pass filter and a notch filter are used on the control input path of the microactuator. The transfer function of these filters is given by

$$H(s) = \frac{1.7766 \times 10^8}{s^2 + 17,910s + 8.883 \times 10^7} \cdot \frac{s^2 + 3456s + 1.194 \times 10^9}{s^2 + 69,120s + 1.194 \times 10^9}, \tag{25}$$

where the first term is a second-order low-pass filter with a cut-off frequency at 1500 Hz and the second term is a notch filter with a center frequency at 5500 Hz. These filters are used to attenuate the microactuator resonant modes and high frequency noises. The frequency response of the microactuator together with these filters given in Fig. 6 clearly shows that the resulting system can be cleanly approximated by a static gain at low frequencies.

3. Following the design procedure given in Section 3 and the physical properties of the VCM actuator, we choose an appropriate state feedback gain,

$$F(\varepsilon) = -\frac{1}{6.4013 \times 10^7} \left[ \frac{4\pi^2 f^2}{\varepsilon^2} \quad \frac{4\pi f \zeta}{\varepsilon} \right], \tag{26}$$

such that the resulting closed-loop system has a low damping ratio  $\zeta = 0.3$  and a natural frequency  $f = 190$  Hz with  $\varepsilon = 1$ . Here we note that  $\varepsilon$  is a tuning parameter, which can be tuned with respect to the amplitude of the command reference  $r$ . Choosing a reduced order observer gain  $K_R = -4000$ , we obtain a reduced order CNF control law as follows:

$$\dot{x}_c = -4000x_c - 1.6 \times 10^7 \hat{y}_v + 6.4013 \times 10^7 \text{sat}(u_v), \tag{27}$$

and

$$u_v = \kappa_2 x_c + (\kappa_1 + 4000\kappa_2) \hat{y}_v - \kappa_1 r + \rho(r, \hat{y}_v) [\kappa_3 x_c + (4000\kappa_3 - \kappa_1) \hat{y}_v + \kappa_1 r], \tag{28}$$

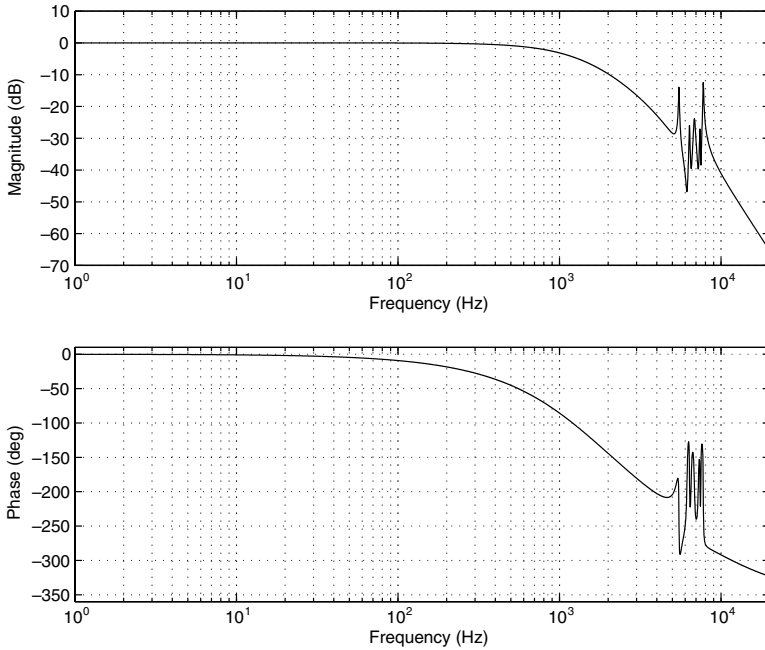


Fig. 6. Frequency response of the microactuator with filters.

where

$$\kappa_1 = -\frac{0.0223}{\varepsilon^2}, \quad \kappa_2 = -\frac{1.119 \times 10^{-5}}{\varepsilon}, \quad \kappa_3 = \frac{3.4191 \times 10^{-5}}{\varepsilon}, \quad (29)$$

and  $\rho(r, \hat{y}_v)$  is as given follows:

$$\rho(r, \hat{y}_v) = -\beta |e^{-\alpha|r-\hat{y}_v|} - 0.3679|, \quad (30)$$

with  $\alpha = 1$ ,  $\beta = 1.582$  and  $\varepsilon = 1$  for  $r = 1 \mu\text{m}$ ;  $\alpha = 0.05$ ,  $\beta = 2.294$  and  $\varepsilon = 1.2258$  for  $r = 20 \mu\text{m}$ ; and  $\alpha = 0.02$ ,  $\beta = 2.373$  and  $\varepsilon = 1.2258$  for  $r = 50 \mu\text{m}$ . The values of these parameters are obtained through simulations. We note that it is simple to interpolate these parameters as some polynomial functions of  $r$ . Thus, there are no difficulties in implementing our control law onto the actual system.

4. Noting the facts that: (i) the model of the microactuator can be approximated as a constant gain, i.e., (5), at low frequency region; (ii) the control input to the microactuator has to be kept within  $\pm 2 \text{ V}$ ; (iii) the maximum displacement of the microactuator is  $1 \mu\text{m}$ ; and (iv) the switch is set to be activated when  $|r - \hat{y}_v| \leq 1.5 \mu\text{m}$ . Theoretically, the gain  $k_s$  should be chosen as 0.5 in order to estimate the displacement of the microactuator. However, our experience shows that it will yield a much better performance by choosing  $k_s = 1$ .

Next, in order to compare the above design with the single-stage servo systems with VCM actuator, a reduced order CNF control law for the VCM actuator is designed as follows:

$$\dot{x}_c = -4000x_c - 1.6 \times 10^7 y_v + 6.4013 \times 10^7 \text{sat}(u_v), \tag{31}$$

and

$$u_v = \kappa_2 x_c + (\kappa_1 + 4000\kappa_2)y_v - \kappa_1 r + \rho(r, y_v)[\kappa_3 x_c + (4000\kappa_3 - \kappa_1)y_v + \kappa_1 r], \tag{32}$$

where

$$\kappa_1 = -\frac{0.0223}{\varepsilon^2}, \quad \kappa_2 = -\frac{1.119 \times 10^{-5}}{\varepsilon}, \quad \kappa_3 = \frac{3.4191 \times 10^{-5}}{\varepsilon}, \tag{33}$$

and  $\rho(r, y_v)$  is as given as follows:

$$\rho(r, y_v) = -\beta |e^{-\alpha|r-y_v|} - 0.3679|, \tag{34}$$

with  $\alpha = 1$ ,  $\beta = 1.582$  and  $\varepsilon = 1$  for  $r = 1 \mu\text{m}$ ;  $\alpha = 0.05$ ,  $\beta = 2.136$  and  $\varepsilon = 1.1875$  for  $r = 20 \mu\text{m}$ ; and  $\alpha = 0.02$ ,  $\beta = 2.215$  and  $\varepsilon = 1.2258$  for  $r = 50 \mu\text{m}$ .

Although our controller is nonlinear in nature, we still manage to obtain the sensitivity and complementary sensitivity functions of the resulting servo systems by focusing on the steady state situation when the nonlinear function  $\rho$  of the CNF controllers can roughly be approximated by a constant. The resulting sensitivity and complementary sensitivity functions are shown in Fig. 7. The resulting gain margins for the single-stage and dual-stage actuated HDD servo systems are respectively

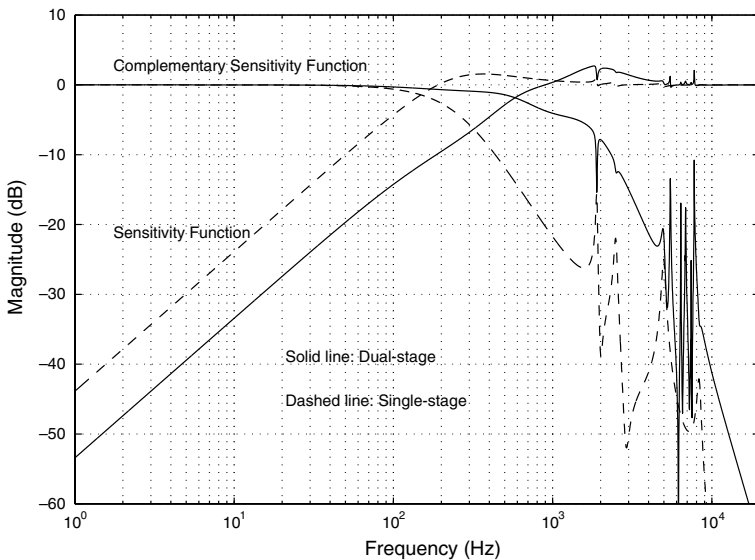


Fig. 7. Sensitivity and complementary sensitivity functions of the servo systems.

given by 6.4 and 6.2 dB, whereas their phase margins are  $52^\circ$  and  $56^\circ$ , respectively. Both controlled systems are acceptable from the practical point of view. The time domain properties of the servo systems are to be evaluated in the next section.

## 5. Simulation and implementation results

The simulation results are done in a continuous-time setting. The implementation results are carried out at a sampling frequency of 20 kHz. We note that the HDD used in our experiment has all its cover and disk plates removed, and is placed on a vibration-free table. The displacement of the R/W head is measured by an LDV, and the real-time control is implemented using a dSpace package. The results of the dual-stage actuated HDD servo system will then be compared with those of the servo system with a single-stage VCM actuator. The latter is done on the same drive by keeping the microactuator inactive throughout the whole implementation process. As expected, and as to be seen soon, the dual-stage actuated servo system yields better performances compared to the single-stage actuated counterpart.

### 5.1. Track seeking and following test

We first test the performance of track seeking and track following of the dual-stage actuated servo system. The simulation and implementation results with various seek lengths, i.e., for  $r = 1$ ,  $r = 20$  and  $50 \mu\text{m}$ , are to be presented. The contributions of the microactuator to the overall response can be clearly observed from these results. Results of the corresponding single-stage actuated system will also be given for comparison. The results of the HDD servo systems are shown in Figs. 8–13. The settling times and the percentages of improvement are summarized in Table 1. Clearly, the results show that the dual-stage actuated servo system yields better performances in both the track seeking and track following stages than the single-stage counterpart.

### 5.2. Position error signal test

The disturbances in a real HDD are usually considered as a lumped disturbance at the plant output, also known as runouts. Repeating runouts (RROs) and non-repeating runouts (NRROs) are the major sources of track following errors. RROs are caused by the rotation of the spindle motor and consists of frequencies that are multiples of the spindle frequency. NRROs can be perceived as coming from three main sources: vibration shocks, mechanical disturbance and electrical noise. Static force due to flex cable bias, pivot-bearing friction and windage are all components of the vibration shock disturbance. Mechanical disturbances include spindle motor variations, disk flutter and slider vibrations. Electrical noises include quantization errors, media noise, servo demodulator noise and power amplifier noise. NRROs are usually random and unpredictable by nature, unlike repeating runouts. They

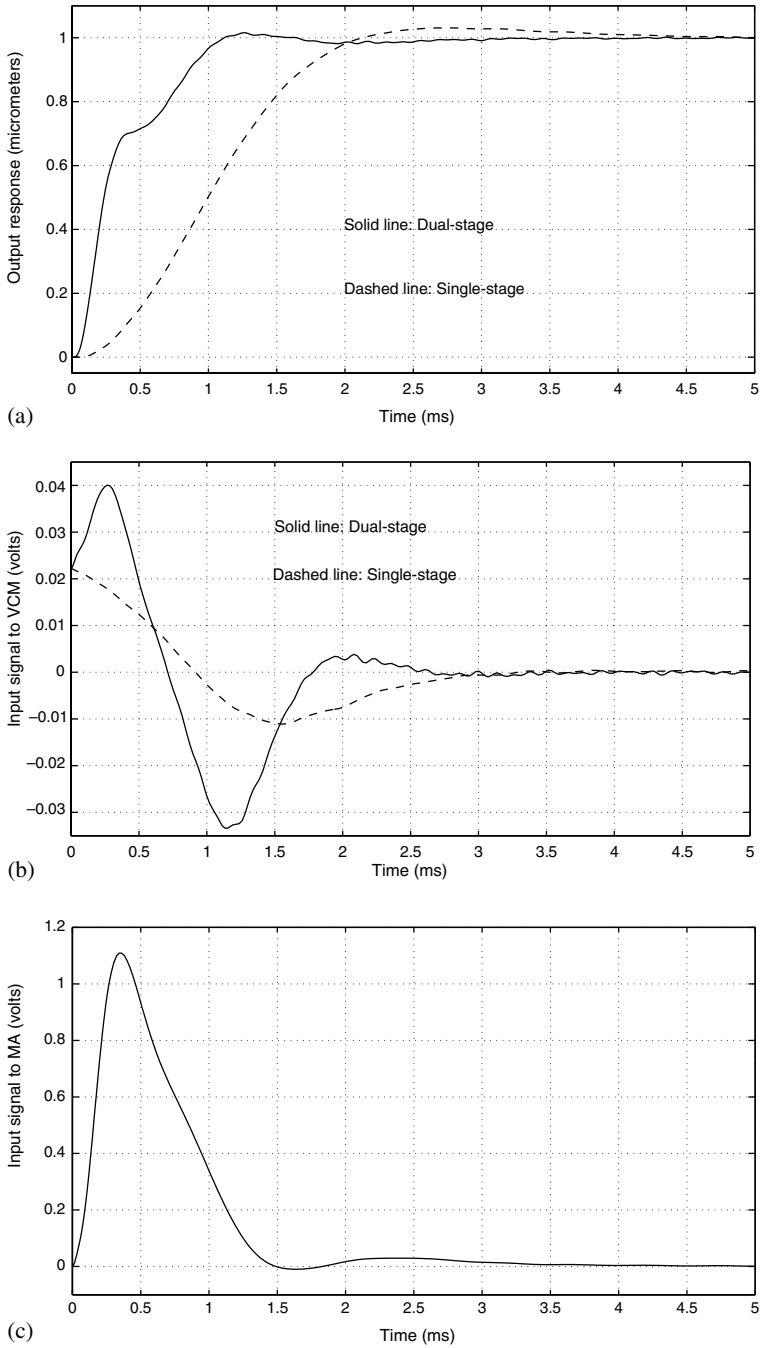


Fig. 8. Simulation results: responses and control signals for  $r = 1 \mu\text{m}$ . (a) Output responses, (b) control signals to VCM actuator, and (c) control signals to microactuator.

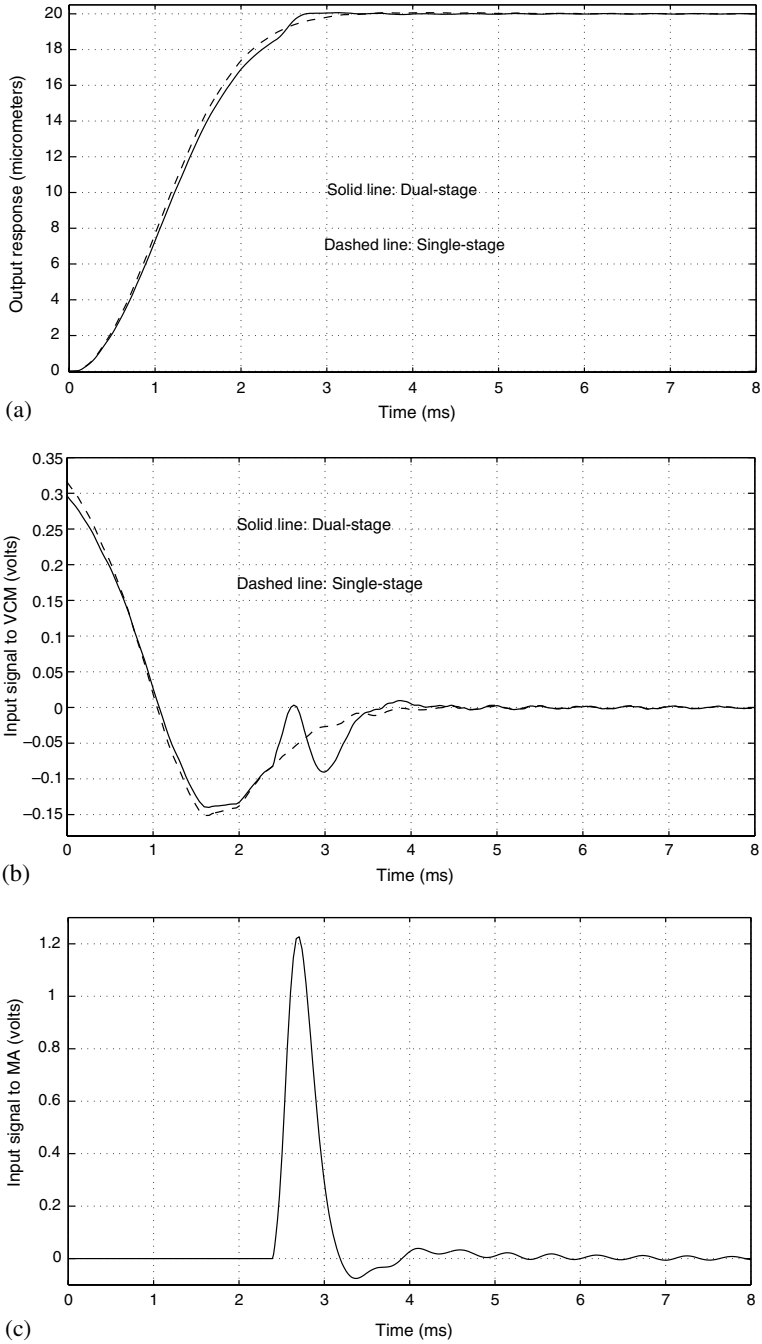


Fig. 9. Simulation results: responses and control signals for  $r = 20 \mu\text{m}$ . (a) Output responses, (b) control signals to VCM actuator, and (c) control signals to microactuator.

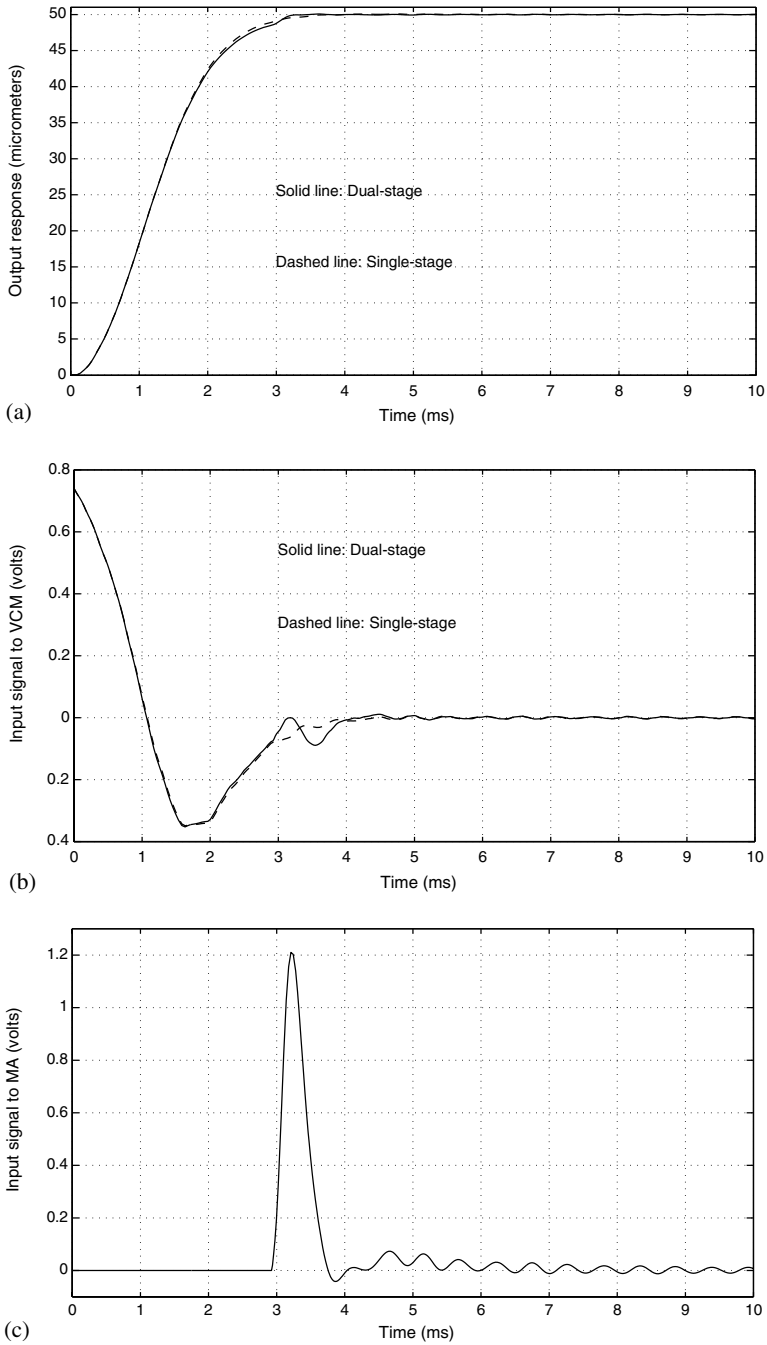


Fig. 10. Simulation results: responses and control signals for  $r = 50 \mu\text{m}$ . (a) Output responses, (b) control signals to VCM actuator, and (c) control signals to microactuator.

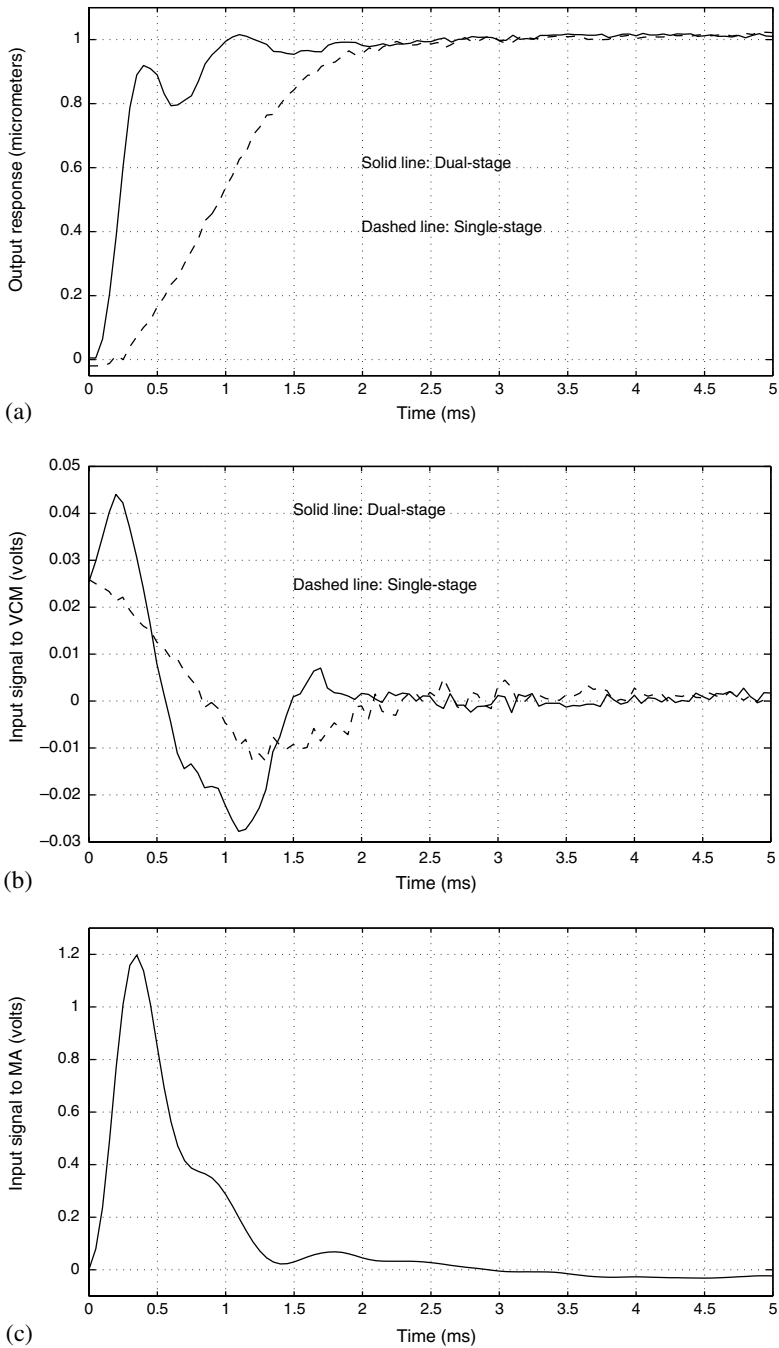


Fig. 11. Experimental results: responses and control signals for  $r = 1 \mu\text{m}$ . (a) Output responses, (b) control signals to VCM actuator, and (c) control signals to microactuator.

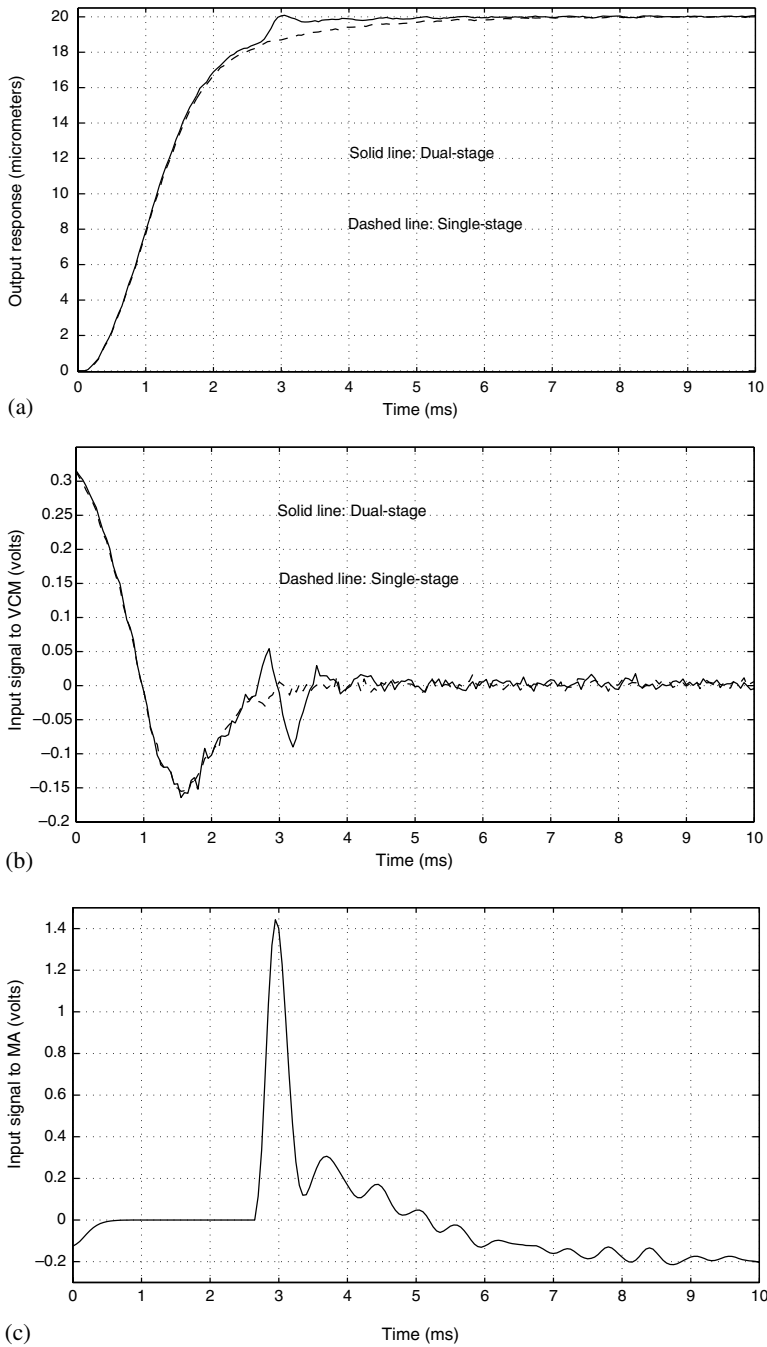


Fig. 12. Experimental results: responses and control signals for  $r = 20 \mu\text{m}$ . (a) Output responses, (b) control signals to VCM actuator, and (c) control signals to microactuator.

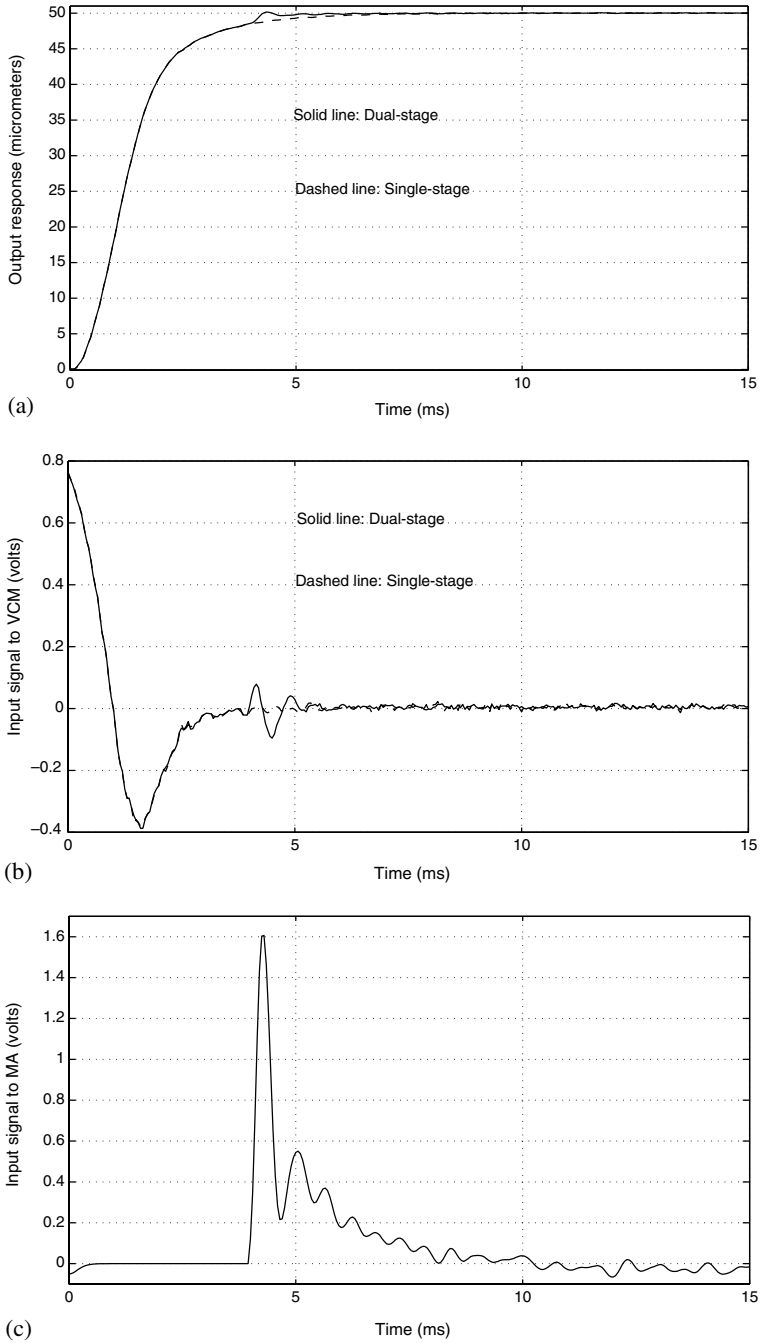


Fig. 13. Experimental results: responses and control signals for  $r = 50 \mu\text{m}$ . (a) Output responses, (b) control signals to VCM actuator, and (c) control signals to microactuator.

Table 1  
Performances of single- and dual-stage HDD servo systems

Target ( $\mu\text{m}$ )	Single	Dual	Improvement (%)
<i>Panel A: Simulation results: settling time (ms)</i>			
1	1.85	0.95	49
20	3.10	2.70	13
50	3.60	3.20	11
<i>Panel B: Experimental results: settling time (ms)</i>			
1	1.9	1.0	47
20	6.5	5.3	18
50	8.2	6.2	24

are also of a lower magnitude (see e.g., [8]). A perfect servo system for HDD should reject both the RROs and NRROs.

As mentioned earlier, the cover and disk plates of the HDD are removed in our experiment. As such, some disturbances of the actual system, e.g., the runout disturbances, are no longer existent. In order to test the robustness of our design against these disturbances, we need to artificially add the runouts and other disturbances into the system. Based on previous experiments, we know that the runouts in real

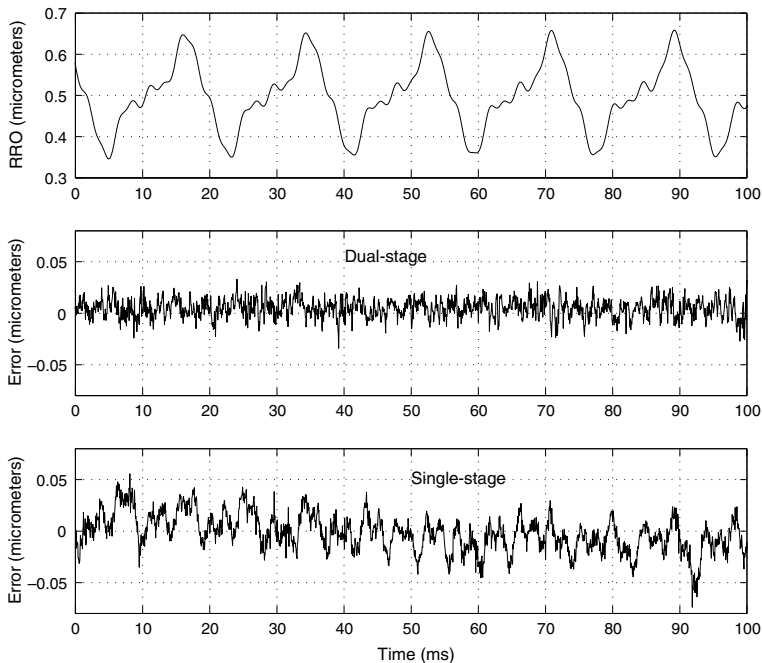


Fig. 14. Implementation results: responses to a runout disturbance.

disk drives are composed mainly of RROs, which are basically sinusoidal with a frequency of about 55 Hz and its multiples, equivalent to the spin rate of the spindle motor. By manually adding this “noise” to the output while keeping the reference signal at zero, we can then read off the subsequent position signal as the expected position error signal (PES) in the presence of runouts. In disk drive applications, the variations in the position of the R/W head from the center of the track during track following, which can be directly read off as the PES, is very important. Track following servo systems have to ensure that the PES is kept to a minimum. Having deviations that are above the tolerance of the disk drive would result in too many read or write errors, making the disk drive unusable. A suitable measure is the standard deviation of the readings, i.e.,  $\sigma_{pes}$ .

We conduct the PES tests for the complete single- and dual-stage actuated servo systems by injecting a fictitious runout signal,

$$w(t) = 0.5 + 0.1 \cos(110\pi t) + 0.05 \sin(220\pi t) + 0.02 \sin(440\pi t) + 0.01 \sin(880\pi t), \tag{35}$$

into the actual system. The unit for  $w(t)$  is in micrometer. The results, i.e., the actual output responses and the histograms of the PES tests, are given in Figs. 14 and 15. The  $3\sigma_{pes}$  values of the PES tests, which are a measure of track mis-registration (TMR) in HDD and which are closely related to the maximum achievable track den-

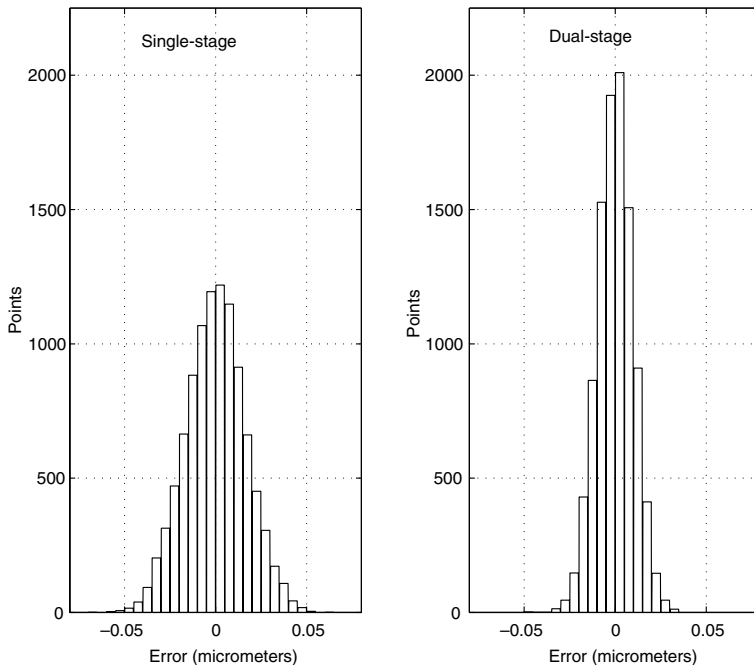


Fig. 15. Implementation results: PES test histograms.

Table 2  
Results of the position error signal (PES) tests

	Single	Dual	Improvement (%)
$3\sigma_{\text{pes}}$ ( $\mu\text{m}$ )	0.049	0.030	39

sity, for the single- and dual-stage actuated servo systems are summarized in Table 2. Clearly, the dual-stage actuated system has outperformed its single-stage counterpart once again.

## 6. Conclusion

We have presented in this paper the design of a dual-stage actuated hard disk servo system using the newly developed CNF control approach. It can be easily observed from the results that the dual-stage actuated servo systems do provide faster responses compared with those of the single-stage actuated counterparts. The improvement in the track following stage turns out to be very noticeable. In particular, the dual-stage actuated HDD system has outperformed the single-stage actuated counterpart very impressively in track following. This was actually the original purpose of introducing the microactuator to HDD servo systems.

## Acknowledgments

The authors would like to thank anonymous reviewers for their constructive comments that have helped a great deal to improve the overall presentation and results of this work.

## References

- [1] Aggarwal SK, Horsley DA, Horowitz R, Pisano AP. Microactuators for high density disk drives. In: Proceedings of American Control Conference, Albuquerque, USA, 1997. p. 3979–84.
- [2] Chen BM, Lee TH, Hang CC, Guo Y, Weerasooriya S. An  $H_\infty$  almost disturbance decoupling robust controller design for a piezoelectric bimorph actuator with hysteresis. *IEEE Trans Control Syst Technol* 1999;7:160–74.
- [3] Chen BM, Lee TH, Venkataramanan V. Hard disk drive servo systems. London: Springer; 2002.
- [4] Chen BM, Lee TH, Peng K, Venkataramanan V. Composite nonlinear feedback control: theory and an application. *IEEE Trans Autom Control* 2003;48:427–39.
- [5] Ding J, Tomizuka M, Numasato H. Design and robustness analysis of dual stage servo system. In: Proceedings of American Control Conference, Chicago, USA, 2000. p. 2605–9.
- [6] Evans RB, Griesbach JS, Messner WC. Piezoelectric microactuator for dual stage control. *IEEE Trans Magn* 1999;35:977–82.
- [7] Eykhoff P. System identification—parameter and state estimation. New York: John Wiley; 1981.
- [8] Franklin GF, Powell JD, Workman ML. Digital control of dynamic systems. 3rd ed. Reading, MA: Addison-Wesley; 1998.

- [9] Guo L, Martin D, Brunnett D. Dual-stage actuator servo control for high density disk drives. In: Proceedings of the 1999 IEEE/ASME International Conference on Advanced Intelligent Mechatronics, Atlanta, USA, 1999. p. 132–7.
- [10] Guo L, Chang JK, Hu X. Track-following and seek/settle control schemes for high density disk drives with dual-stage actuators. In: Proceedings of the 2001 IEEE/ASME International Conference on Advances Intelligent Mechatronics, Como, Italy, 2001. p. 1136–41.
- [11] Guo W, Weerasooriya S, Goh TB, Li QH, Bi C, Chang KT et al. Dual stage actuators for high density rotating memory devices. *IEEE Trans Magn* 1998;34:450–5.
- [12] Guo W, Yuan L, Wang L, Guo G, Huang T, Chen BM, et al. Linear quadratic optimal dual-stage servo control systems for hard disk drives. In: Proceedings of the 24th Annual Conference of the IEEE Industrial Electronics Society, vol. 3, Aachen, Germany, August 1998. p. 1405–10.
- [13] Hernandez D, Park SS, Horowitz R, Packard AK. Dual-stage track-following servo design for hard disk drive. In: Proceedings of American Control Conference, San Diego, CA, USA, 1999. p. 4116–21.
- [14] Horsley DA, Hernandez D, Horowitz R, Packard AK, Pisano AP. Closed-loop control of a microfabricated actuator for dual-stage hard disk drive servo systems. In: Proceedings of American Control Conference, Philadelphia, USA, 1998. p. 3028–32.
- [15] Hu X, Guo W, Huang T, Chen BM. Discrete time LQG/LTR dual-stage controller design and implementation for high track density HDDs. In: Proceedings of American Control Conference, San Diego, CA, USA, 1999. p. 4111–5.
- [16] Kobayashi M, Horowitz R. Track seek control for hard disk dual-stage servo systems. *IEEE Trans Magn* 2001;37:949–54.
- [17] Li Y, Horowitz R. Track-following controller design of MEMS based dual-stage servos in magnetic hard disk drives. In: Proceedings of the 2000 IEEE International Conference on Robotics and Automation, San Francisco, USA, 2000. p. 953–8.
- [18] Lin Z, Pachter M, Banda S. Toward improvement of tracking performance—nonlinear feedback for linear systems. *Int J Control* 1998;70:1–11.
- [19] Mori K, Munemoto T, Otsuki H, Yamaguchi Y, Akagi K. A dual-stage magnetic disk drive actuator using a piezoelectric device for a high track density. *IEEE Trans Magn* 1991;27:5298–300.
- [20] Oboe R, Beghi A, Murari B. Modeling and control of a dual stage actuator hard disk drive with piezoelectric secondary actuator. In: Proceedings of the 1999 IEEE/ASME International Conference on Advanced Intelligent Mechatronics, Atlanta, USA, 1999. p. 138–43.
- [21] Schroeck SJ, Messner WC. On controller design for linear time-invariant dual-input single output systems. In: Proceedings of American Control Conference, San Diego, USA, 1999. p. 4122–6.
- [22] Semba T, Hirano T, Hong J, Fan LS. Dual-stage servo controller for HDD using MEMS microactuator. *IEEE Trans Magn* 1999;35:2271–3.
- [23] Takaishi K, Imamura T, Mizasgita Y, Hasegawa S, Ueno T, Yamada T. Microactuator control for disk drive. *IEEE Trans Magn* 1996;32:1863–6.
- [24] Wang L, Yuan L, Chen BM, Lee TH. Modeling and control of a dual-stage servo system for hard disk drives. In: Proceedings of the 1998 International Conference on Mechatronics Technology, Hsinchu, Taiwan, 1998. p. 533–8.
- [25] Workman ML. Adaptive proximate time optimal servomechanisms. PhD Dissertation, Stanford University, 1987.